Noname manuscript No.
(will be inserted by the editor)

Kovasznay Mode Decomposition of Velocity-Temperature Correlation in Canonical Shock-Turbulence Interaction

Russell Quadros, Krishnendu Sinha and Johan Larsson

Received: date / Accepted: date

Abstract The correlation coefficient R_{uT} between the streamwise velocity and the temperature is investigated for the case of canonical shock-turbulence interaction, motivated by the fact that this correlation is an important component in compressible turbulence models. The variation of R_{uT} with the Mach number, turbulent Mach number, and the Reynolds number is predicted using linear inviscid theory and compared to data from DNS. The contributions from the individual Kovasznay modes are quantified. At low Mach numbers, the peak post-shock R_{uT} is determined by the acoustic mode, which is correctly predicted by linear theory. At high Mach numbers, it is determined primarily by the vorticity and entropy modes, which are more strongly affected by nonlinear and viscous effects, and thus less well predicted by linear theory.

Keywords Turbulent heat flux · Linear interaction analysis · Direct numerical simulation data · Vorticity · Entropy · Acoustic

1 Introduction

A shock wave impinging on a supersonic boundary layer may lead to the separation and reattachment of the boundary layer, which in turn causes a high localized heat transfer to the surface [9, 2]. When the incoming boundary

R. Quadros and K. Sinha:
Department of Aerospace Engineering,
Indian Institute of Technology Bombay,
Mumbai 400076, India.
E-mail: krish@aero.iitb.ac.in

J. Larsson:
Department of Mechanical Engineering,
University of Maryland, College Park,
Maryland 20742, USA.

layer is turbulent, the peak heat transfer around the shock can be an order of magnitude higher than that in the incoming flow [19].

Engineering predictions of shock/boundary-layer interaction (SBLI) in practical configurations rely on the Reynolds-averaged Navier Stokes approach. An important unclosed term in the mean energy conservation equation is the turbulent enthalpy flux $\widetilde{u_j''h''}$ or the turbulent heat flux $\widetilde{u_j''T''}$, where u_j is the velocity in the j^{th} direction, h is the enthalpy and T is the temperature of the gas. The tilde represents Favre (density-weighted) averaging, with the corresponding fluctuations marked by a double prime.

The turbulent heat flux is conventionally modelled using the gradient-diffusion hypothesis, i.e., as a turbulent conductivity k_T multiplied by the gradient of the mean temperature. The turbulent conductivity k_T is then related to the eddy viscosity μ_T via a turbulent Prandtl number $Pr_T = c_p\mu_T/k_T$. The standard modelling approach is to follow the strong Reynolds analogy proposed by [14] and assume that the velocity and temperature fluctuations are anti-correlated, i.e., that the correlation coefficient

$$R_{uT} = \frac{\widetilde{u''T''}}{\sqrt{\widetilde{u''^2}}\sqrt{\widetilde{T''^2}}} \tag{1}$$

is equal to -1. This assumption corresponds to a value of the turbulent Prandtl number $Pr_T = 1$ [23]; in practice, a constant value of $Pr_T = 0.89$ gives satisfactory results in flat plate boundary-layer flows and is often used in SBLI applications.

The strong Reynolds analogy assumes that the total temperature fluctuations in a flow are negligible compared to the fluctuations in the static temperature and the flow kinetic energy. This is not true in the presence of shock waves. For example, Mahesh et al [12] showed that considerable total temperature fluctuations are generated in the vicinity of a shock. As a consequence, they found that R_{uT} varied significantly across and behind the shock. The variation in R_{uT} could imply that the turbulent Prandtl number Pr_T used in standard models should vary around a shock as well. Indeed, some variable-Pr_T models have been found to improve the peak surface heat flux prediction in SBLI compared to conventional models [25].

A thorough study of R_{uT} is therefore important for high-speed flows with shock waves, and is the focus of the current work. Specifically, the objective is to study the variation of R_{uT} with flow parameters like the shock strength (characterized by the upstream mean Mach number M_{in}), the turbulence intensity (characterized by the turbulent Mach number $M_{t,\text{in}}$), and the Reynolds number Re (that characterizes viscous effects). We also consider different types of inflow disturbance fields, namely, vorticity, entropy, acoustic and their combination. Most importantly, understanding the physics that determine R_{uT} and its variation downstream of the shock could provide crucial insight towards developing closure models for the turbulent heat flux in the shock region.

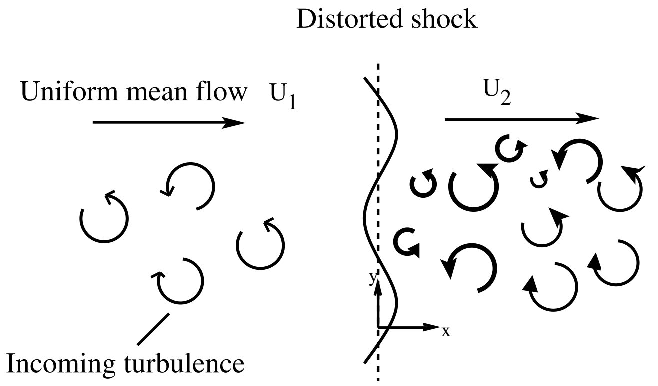

Fig. 1 Schematic of shock-turbulence interaction (STI), showing how incoming turbulence is convected through a normal shock wave located at $x = 0$. The shock gets distorted about its mean location, and the turbulence is amplified as it passes through the shock.

In this work, we study the evolution of R_{uT} in a canonical shock-turbulence interaction (STI), which consists of homogeneous isotropic turbulence passing through a nominally normal shock wave as shown in figure 1. This is a scenario where the effect of the shock wave on the turbulence can be studied in isolation, while other effects important in SBLI (such as mean shear, flow separation and attachment, and streamline curvature) are eliminated. In spite of the simplicity, the model problem exhibits a range of physical effects, including turbulence anisotropy, generation of acoustic waves, baroclinic torques, and unsteady shock oscillations. A significant amount of direct numerical simulation (DNS) data is also available [6, 20] for this canonical configuration for various mean and turbulent Mach numbers as well as Reynolds numbers.

The current study relies on the linear interaction analysis (LIA), pioneered by Ribner [17, 18], in which the turbulence is modelled as an infinitesimal perturbation around an inviscid shock wave, and where the post-shock evolution is assumed to be linear and inviscid. The accuracy of LIA has been assessed in comparisons with high-fidelity computations since the early 1990s [7, 8, 3, 12, 4]. In a particularly convincing study, Ryu and Livescu [20] showed that the post-shock Reynolds stresses in DNS converge towards the LIA prediction as the turbulence intensity ($\sim M_{t,\mathrm{in}}/M_{\mathrm{in}}$) goes to zero, even at low Reynolds numbers. In addition, Larsson et al [6] showed that the trace (but not the anisotropy) of the post-shock Reynolds stresses in DNS agrees quite well with the LIA predictions even for large turbulence intensities, provided that the post-shock viscous decay in DNS was compensated for.

In a recent work, Quadros et al [16] studied the turbulent energy flux $\widetilde{u''e''}$ in canonical shock-turbulence interaction, where e'' is the fluctuation in the internal energy. This correlation is proportional to $\widetilde{u''T''}$ for a calorically perfect gas. They presented detailed comparison of the LIA results with available DNS data for the turbulent energy flux, and analyzed the budget of the $\widetilde{u''e''}$ transport equation behind the shock to elucidate the underlying physics. They found that the post-shock evolution of the turbulent energy flux is primarily governed by the linear inviscid mechanisms, while direct effects of viscosity, conductivity and turbulent transport are small.

The current work takes a different approach. The physics of the problem is studied in terms of the three Kovasznay modes of vorticity, entropy and acoustic disturbances that form the basis of the linear interaction analysis. The contributions of the three modes to the velocity-temperature correlation generated at the shock are computed from the linear theory. The LIA prediction of the individual modes are also computed and compared to available DNS data. It is found that the acoustic mode is predicted better than the others, and the R_{uT} values determined by the acoustic mode are reproduced well by LIA. Other aspects dominated by the vorticity and entropy modes are not predicted correctly. The current results thus complement those presented in Quadros et al [16], and bring out a different aspect of the physics involved in the shock-turbulence interaction. In addition, the extensive R_{uT} data presented here are of direct relevance towards modelling turbulent heat flux, specifically in terms of a variable turbulent Prandtl number.

2 Problem formulation and the linear interaction analysis (LIA)

Linear interaction analysis models the turbulence as a superposition of two-dimensional planar waves (Fourier modes) with varying wavenumbers and frequencies, each independently interacting with the shock. One such interaction is schematically shown in figure 2, where the upstream vortical wave is characterized by a wavenumber k, an angle of incidence ψ and a complex amplitude A_v. Under the assumption of small disturbances and inviscid flow, the fluctuations in the regions both upstream and downstream of the shock are governed by linearized Euler equations. The description below follows the work of Mahesh et al [11], with the parts that are directly relevant to the current work presented for completeness. A different, more compact, formulation of LIA can be found in Fabre et al [1].

The upstream velocity fluctuations are taken as

$$\frac{u_1'}{U_1} = A_v \sin\psi \exp[ik(x\cos\psi + y\sin\psi - U_1 t\cos\psi)], \tag{2a}$$

$$\frac{v_1'}{U_1} = -A_v \cos\psi \exp[ik(x\cos\psi + y\sin\psi - U_1 t\cos\psi)], \tag{2b}$$

where u' and v' are the velocities in the streamwise (x) and transverse (y) directions, the subscript 1 corresponds to a state upstream of the shock, U denotes the streamwise mean velocity, and t is time. The incoming fluctuations in pressure (p_1'), density (ρ_1') and temperature (T_1') are related to the incoming entropy and acoustic waves. The shock distorts from its mean position by a distance $x = \xi(y,t)$ upon interaction.

The interaction of an incident wave - vorticity, entropy or acoustic - generates waves of all three kinds behind the shock. The post-shock fluctuations

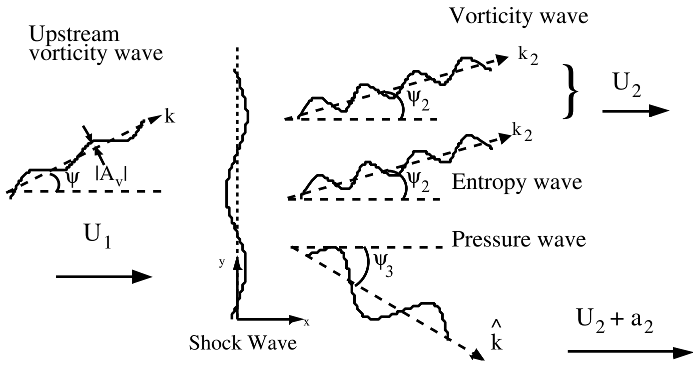

Fig. 2 A single incoming vortical wave carried by a uniform mean flow velocity U_1 interacts with a normal shock to generate vorticity, entropy and acoustic waves downstream of the shock. The vorticity and entropy waves are carried by the downstream mean flow velocity U_2, and the acoustic wave is carried at the speed of sound a_2 relative to the mean velocity.

are obtained by substituting the downstream waveforms in the linearized Euler and the linearized Rankine-Hugoniot equations, and solving the resulting set of linear algebraic equations. The post-shock turbulent heat flux can then be computed from the downstream fluctuations.

$$\overline{u_2' T_2'} = \frac{1}{2}\left[\overline{u_2' T_2'^*} + \overline{T_2' u_2'^*}\right], \tag{3}$$

where * indicates a complex conjugate and subscript 2 corresponds to the post-shock state. Similar expressions for $\overline{u'^2}$ and $\overline{T'^2}$ can be written, and the value of R_{uT} can thus be found using (1). Note that the difference between Reynolds- and Favre-averaging is negligible in the linear framework.

Three-dimensional turbulence is modelled as a collection of two-dimensional elementary waves satisfying a prescribed energy spectrum [18]. For an upstream isotropic spectrum consisting of vorticity/entropy waves, the downstream turbulent heat flux is

$$(\overline{u_2' T_2'})_{3D} = 4\pi \int_{\psi=0}^{\pi/2} \int_{k=0}^{\infty} (\overline{u_2' T_2'})_{2D}\; k^2 \;\sin\psi \; dk\; d\psi\,, \tag{4}$$

where ϕ is the azimuthal angle, and $(\overline{u_2' T_2'})_{2D}$ is the correlation obtained for a two-dimensional planar wave given by (3). Similar results for $(\overline{u_2' u_2'})_{3D}$ and $(\overline{T_2' T_2'})_{3D}$ can be obtained to compute R_{uT}. All the results presented in the current work are for the three-dimensional interaction, and the subscript $3D$ is avoided for convenience.

The amplitude of the upstream velocity disturbance $|A_v|$ is related to the energy spectrum as

$$|A_v|^2 = \frac{E(k)}{4\pi k^2},$$

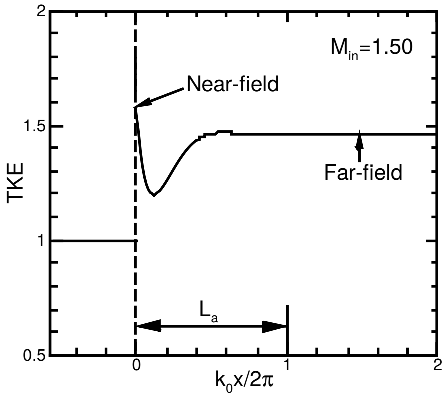

Fig. 3 Streamwise variation of turbulence kinetic energy as predicted by LIA for purely vortical isotropic turbulence interacting with a $M_{\text{in}} = 1.5$ normal shock. The TKE is normalized by its upstream value, and the streamwise distance is normalized by $2\pi/k_o$, which is the wavelength corresponding to the peak upstream energy level. The shock is located at $x = 0$, and the near-field, the far-field and the acoustic adjustment region L_a are shown.

where $E(k)$ is the three-dimensional energy spectrum taken as [15]

$$E(k) \sim \frac{\left(\frac{k}{k_0}\right)^2}{\left[\left(\frac{k}{k_0}\right)^2 + \frac{5}{6}\right]^{\frac{11}{6}}}, \tag{5}$$

where k_0 is the wavenumber corresponding to the peak energy. The sensitivity of the LIA predictions to the exact shape of the spectrum was studied in Quadros et al [16]: provided that the spectrum had a broadband character, the exact shape was not found to be crucial.

A representative three-dimensional LIA result for the streamwise variation of the turbulence kinetic energy (TKE) is shown in figure 3, where the upstream turbulence is purely vortical. The point just across the shock ($x = 0^+$) is referred to as the near-field. This is followed by an adjustment region of length L_a (about one large eddy scale), followed by the far-field in which the LIA prediction is constant.

3 Post-shock R_{uT} for purely vortical upstream turbulence

We start by studying the post-shock R_{uT} correlation coefficient generated by the special case of purely vortical incoming disturbances. Therefore, in this section only, the fluctuations in pressure, density and temperature are assumed to be zero upstream of the shock.

The streamwise variation of R_{uT} obtained from LIA is shown in figure 4(a) for a sample case. The shock is located at $x = 0$, and R_{uT} is zero upstream of

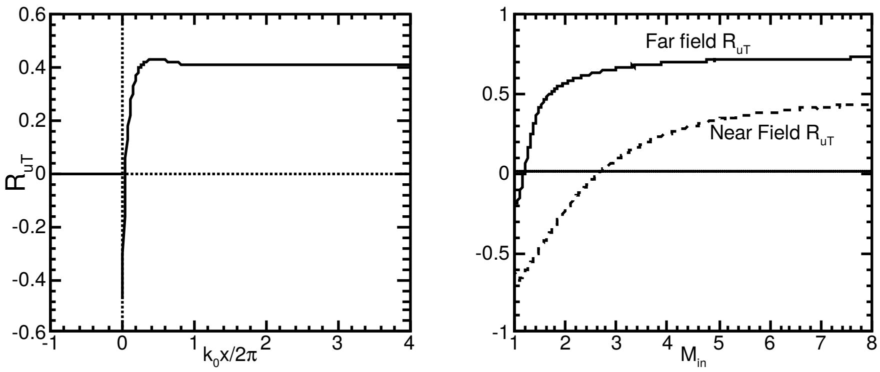

(a) (b)

Fig. 4 LIA prediction of R_{uT} for a purely vortical isotropic turbulence interacting with a normal shock: (a) streamwise variation for $M_{\text{in}} = 1.5$, and (b) near-field and far-field values for varying upstream Mach number.

the shock due to the absence of temperature fluctuations in the incoming flow. Just downstream of the shock, the correlation coefficient attains a negative value, and rapidly rises to a positive peak followed by a constant far-field value. The change in sign is similar to that observed by Quadros et al [16] for the turbulent energy flux, and can be attributed to the decay behind a shock wave.

The decay of the acoustic energy leading to a rapid rise in the turbulent statistics, is an important aspect of shock-turbulence interaction. While this decay leads to a non-monotonic increase in TKE behind the shock, it exponentially decreases the value of thermodynamic fluctuations such as pressure, density and temperature [12]. The acoustic wave generated at the shock will propagate or decay exponentially depending on the upstream incidence angle of each elementary wave [17].

Figure 4(b) shows the near- and far-field values of R_{uT} for varying upstream Mach numbers. For any given Mach number, the far-field value is higher than the near-field value. For upstream Mach numbers $M_{\text{in}} < 2.6$, the near-field R_{uT} values are negative and steadily attain positive values for higher Mach numbers, saturating at about 0.4. The far-field R_{uT} is positive for most Mach numbers and saturates early to a value of about 0.7.

3.1 Comparison between LIA and DNS

Larsson et al [6] performed DNS of canonical shock-turbulence interaction for 20 different cases spanning $M_{\text{in}} = 1.05 - 6$, $M_{t,\text{in}} = 0.05 - 0.38$, and $Re_{\lambda,\text{in}}$ (based on the Taylor-scale) of either 40 or 75; these cases are listed in table 1. The incoming turbulence was largely vortical in DNS, with small

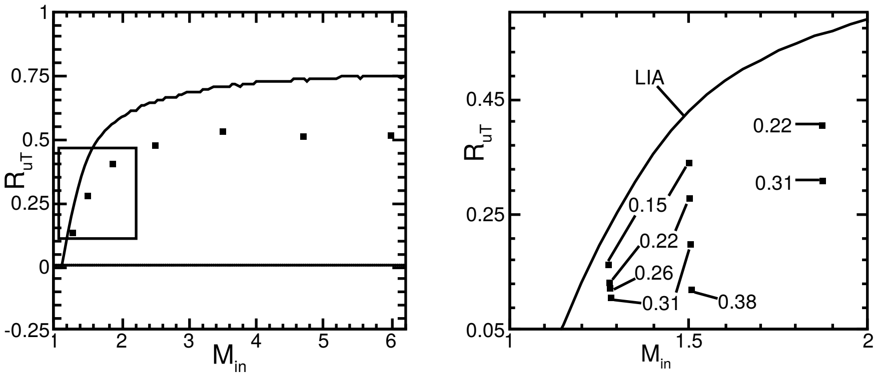

Fig. 5 Comparison of the peak post-shock R_{uT} between LIA (line; purely vortical incoming disturbances) and DNS (symbol) for varying upstream Mach numbers. The DNS cases in (a) correspond to $M_{t,\text{in}} = 0.22$ and $Re_{\lambda,\text{in}} = 40$. Figure (b) shows the effect of $M_{t,\text{in}}$ for a subset of M_{in}.

Table 1 List of the DNS cases from Larsson et al [6] used in the present study. The values correspond to location immediately upstream of the mean shock wave. The peak energy wavenumber k_0 is used to normalize the dissipation length scale L_ϵ.

M_{in}	$M_{t,\text{in}}$	$Re_{\lambda,\text{in}}$	$R_{kk}/(2U_1^2)$	$k_0 L_\epsilon$
1.05	0.05	39	1.1×10^{-3}	3.9
1.28	0.15	38	7.3×10^{-3}	3.9
1.28	0.22	39	7.3×10^{-3}	3.9
1.28	0.26	38	7.3×10^{-3}	4.0
1.28	0.31	38	7.3×10^{-3}	3.8
1.50	0.15	38	5.3×10^{-3}	3.9
1.50	0.22	39	5.3×10^{-3}	4.3
1.50	0.31	39	5.3×10^{-3}	4.1
1.50	0.37	39	5.3×10^{-3}	4.2
1.87	0.22	39	6.9×10^{-3}	3.8
1.87	0.31	39	6.9×10^{-3}	4.0
2.50	0.22	40	4.0×10^{-3}	4.3
3.50	0.16	40	2.1×10^{-3}	4.1
3.50	0.23	41	2.1×10^{-3}	4.3
4.70	0.23	42	1.2×10^{-3}	4.3
6.00	0.23	42	0.7×10^{-3}	4.4
1.50	0.14	73	4.7×10^{-3}	3.0
1.50	0.22	73	11×10^{-3}	2.8
1.50	0.38	72	34×10^{-3}	2.8
3.50	0.15	74	0.9×10^{-3}	2.9

thermodynamic fluctuations upstream of the shock. We compare the DNS data with the LIA predictions to highlight the key physics of the interaction.

Figure 5(a) shows that the DNS post-shock peak R_{uT} follows the same trend as in LIA. Starting from low values, it increases with Mach number to reach an asymptotic level in the hypersonic limit. The linear theory predictions

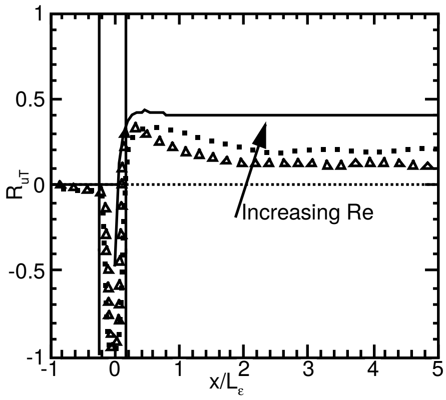

Fig. 6 Streamwise comparison of R_{uT} between LIA (line; purely vortical incoming disturbances) and DNS (symbols) at $M_{\rm in} = 1.50$. The DNS cases have $M_{t,\rm in} = 0.15$ and $Re_{\lambda,\rm in}$ of 40 (triangle) and 75 (square). The vertical lines show the region over which the shock oscillates.

are higher than the DNS data, with a maximum difference of about 30% at high Mach numbers. The difference is highly dependent on the turbulent Mach number $M_{t,\rm in}$ (or, analogously, on the turbulence intensity $\sim M_{t,\rm in}/M_{\rm in}$), as is clearly seen in figure 5(b). The fact that R_{uT} in DNS seem to converge towards the LIA predictions is analogous to the situation in Ryu and Livescu [20], although the present results do not actually reach the LIA result due to the high turbulence intensities. It is also consistent with the observations about the post-shock viscous decay in Larsson et al [6], specifically that viscous decay appears more rapidly for higher $M_{t,\rm in}$ when plotted versus a shock-normal coordinate that is scaled by a large eddy size. In other words, the systematic deviations at higher $M_{t,\rm in}$ in the figure may be due to larger relative viscous effects.

To assess the importance of the Reynolds number, the streamwise profiles of R_{uT} at fixed $M_{\rm in}$ and $M_{t,\rm in}$ but different Reynolds numbers are shown in figure 6. The DNS results clearly approach the LIA prediction at the higher Reynolds number, and the far-field value of R_{uT} is clearly affected by the Reynolds number in DNS. In contrast, the post-shock peak is barely different between the two cases; this could suggest that there is little Re-effect on the peak value, but could also be due to the rather different energy spectra in the two DNS cases. Either way, we conclude that LIA predicts the post-shock peak of R_{uT} rather well for purely vortical incoming disturbances.

We note that the streamwise coordinate is normalized by the dissipation length scale L_ϵ in this figure (and in other figures below). This is calculated just upstream of the shock as

$$L_\epsilon = (R_{kk}/2)^{3/2}/\epsilon,$$

where $R_{kk}/2$ is the turbulence kinetic energy and ϵ is the turbulence dissipation rate. The values of L_ϵ used for normalization are listed in table 1. Due to the absence of viscous dissipation in the linear theory, the most energetic wavenumber (k_0) in the upstream turbulence is used to obtain the characteristic length. It is converted to an equivalent dissipation length scale for LIA using the value of $k_o L_\epsilon \approx 3-4$ found in the DNS data (Larsson et al. 2013). The rather low value (compared to a von Karman spectrum, for example) is likely due to the limited computational box size and the low Reynolds number.

3.2 Modal analysis

To analyze the post-shock R_{uT} results more deeply, we study the individual contributions to the correlation from the different Kovasznay modes. In the LIA formulation, the post-shock velocity fluctuations have contributions from the acoustic and vorticity modes, while the post-shock temperature and density fluctuations have contribution from the acoustic and entropy modes. The pressure fluctuations are purely acoustic. The downstream waveforms can therefore be expressed as

$$\frac{u_2'}{U_1} = A_v \left\{ \hat{F} \exp(i\hat{k}x) + \hat{G} \exp(ikrx\cos\psi) \right\} \exp[ik(y\sin\psi - U_1 t\cos\psi)], \tag{6a}$$

$$\frac{v_2'}{U_1} = A_v \left\{ \hat{H} \exp(i\hat{k}x) + \hat{I} \exp(ikrx\cos\psi) \right\} \exp[ik(y\sin\psi - U_1 t\cos\psi)], \tag{6b}$$

$$\frac{T_2'}{\overline{T}_2} = A_v \left\{ \frac{\gamma-1}{\gamma} \hat{K} \exp(i\hat{k}x) - \hat{Q} \exp(ikrx\cos\psi) \right\} \exp[ik(y\sin\psi - U_1 t\cos\psi)], \tag{6c}$$

$$\frac{\rho_2'}{\overline{\rho}_2} = A_v \left\{ \frac{\hat{K}}{\gamma} \exp(i\hat{k}x) + \hat{Q} \exp(ikrx\cos\psi) \right\} \exp[ik(y\sin\psi - U_1 t\cos\psi)] \tag{6d}$$

$$\frac{p_2'}{P_2} = A_v \left\{ \hat{K} \exp(i\hat{k}x) \right\} \exp[ik(y\sin\psi - U_1 t\cos\psi)], \tag{6e}$$

where P, $\overline{T}$ and $\overline{\rho}$ are the mean pressure, temperature and density, respectively, and γ is the ratio of the specific heats ($\gamma = 1.4$ in this study). The mean density ratio across the shock is r, and $\hat{k}$ denotes the streamwise component of the acoustic mode wavenumber. The complex coefficients $\hat{F}$, $\hat{H}$ and $\hat{K}$ correspond to the acoustic mode, $\hat{G}$ and $\hat{I}$ correspond to the vortical mode and $\hat{Q}$ is associated with the entropy mode.

The velocity-temperature correlation coefficient has contributions from all three modes. The post-shock heat flux can be written in terms of its components using (3) and (6) as

$$\overline{u_2'T_2'} = \left(\overline{u_2'T_2'}\right)_{aa} + \left(\overline{u_2'T_2'}\right)_{ae} + \left(\overline{u_2'T_2'}\right)_{va} + \left(\overline{u_2'T_2'}\right)_{ve}, \tag{7}$$

where the subscripts aa, ae, va and ve correspond to acoustic-acoustic, acoustic-entropy, vortical-acoustic and vortical-entropy components, respectively. The individual contributions are

$$\left(\overline{u_2'T_2'}\right)_{aa} = \frac{1}{2}\frac{\gamma-1}{\gamma}(\hat{F}\hat{K}^* + \hat{K}\hat{F}^*)\exp[i(\hat{k}-\hat{k}^*)x], \tag{8a}$$

$$\left(\overline{u_2'T_2'}\right)_{ae} = -\frac{1}{2}\left[\hat{F}\hat{Q}^*\exp[i(\hat{k}-kr\cos\psi)x] + \hat{Q}\hat{F}^*\exp[i(kr\cos\psi-\hat{k}^*)x]\right], \tag{8b}$$

$$\left(\overline{u_2'T_2'}\right)_{va} = \frac{1}{2}\frac{\gamma-1}{\gamma}\left[\hat{K}\hat{G}^*\exp[i(\hat{k}-kr\cos\psi)x] + \hat{G}\hat{K}^*\exp[i(kr\cos\psi-\hat{k}^*)x]\right], \tag{8c}$$

$$\left(\overline{u_2'T_2'}\right)_{ve} = -\frac{1}{2}\left[\hat{G}\hat{Q}^* + \hat{Q}\hat{G}^*\right]. \tag{8d}$$

Similarly, the post-shock values of $\overline{u'^2}$ and $\overline{T'^2}$ can be written in terms of their Kovasznay mode components as

$$\overline{u_2'u_2'} = \left(\overline{u_2'u_2'}\right)_{aa} + \left(\overline{u_2'u_2'}\right)_{vv} + 2\left(\overline{u_2'u_2'}\right)_{va} \tag{9}$$

and

$$\overline{T_2'T_2'} = \left(\overline{T_2'T_2'}\right)_{aa} + \left(\overline{T_2'T_2'}\right)_{ee} + 2\left(\overline{T_2'T_2'}\right)_{ae}, \tag{10}$$

where the subscripts vv and ee correspond to vortical-vortical and entropy-entropy components. Similarly to (8), the expressions for each of these modal components can be derived from (6).

Figure 7 shows the modal contributions to $\overline{u'T'}$, $\overline{u'^2}$ and $\overline{T'^2}$ for an upstream Mach number $M_{\text{in}} = 1.5$ as predicted by LIA. For each of the correlations, the components associated with the acoustic mode have significant contribution in the region close to the shock. This is most prominent for $\overline{T'^2}$, which takes large values immediately behind the shock and decays rapidly to low levels in the far-field. The temperature fluctuations thus clearly follow the acoustic components in figure 7(c). For the streamwise Reynolds stress, the acoustic and vorticity contributions are negatively correlated. A decay of the acoustic mode therefore results in a rise in $\overline{u'^2}$, as shown in figure 7(b). A similar trend is observed for $\overline{u'T'}$, where competing effects between the acoustic mode correlations results in a local peak in the turbulent heat flux correlation.

Figure 8 quantifies the percentage contribution of the Kovasznay modes to the near-field R_{uT} at varying upstream Mach numbers. At low Mach numbers, the acoustic-acoustic component has a large contribution to $\overline{u'T'}$ and $\overline{T'^2}$. By comparison, the vortical-entropy component of $\overline{u'T'}$ shows a steady buildup from zero at $M_{\text{in}} = 1$ to being the largest contributor beyond Mach 3. The entropy-entropy component of $\overline{T'^2}$ exhibits a similar variation for higher Mach numbers ($M_{\text{in}} > 5.5$).

The modal decomposition of the velocity variance shows a slightly different trend. The vortical-vortical component of $\overline{u'^2}$ is the largest contributor at low Mach numbers, being the only contributor at $M_{\text{in}} = 1$. This is because the

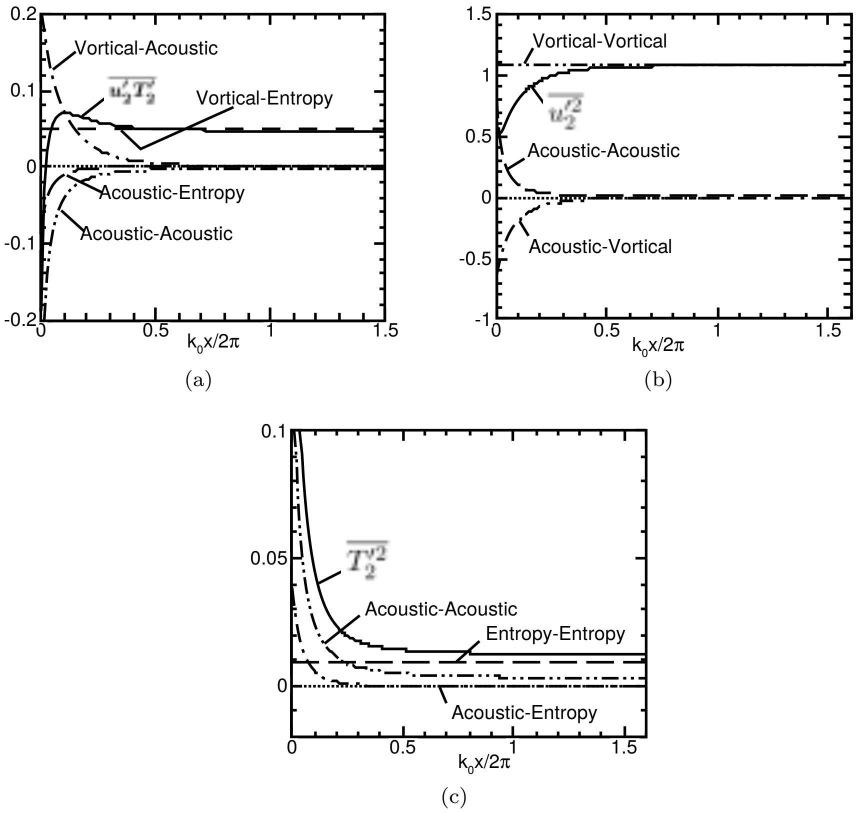

Fig. 7 Kovasznay mode decomposition of (a) $\overline{u'T'}$, (b) $\overline{u'^2}$ and (c) $\overline{T'^2}$ plotted along the streamwise direction for $M_{\rm in} = 1.50$. The upstream turbulence is purely vortical. The velocity fluctuations are normalized by the upstream mean velocity, and the temperature fluctuations are normalized by the downstream mean temperature. All correlations are further normalized by the upstream TKE.

upstream turbulence is purely vortical and remains unchanged across a very weak shock. The contribution of the vortical-vortical component decreases with Mach number, but remains one of the main contributors to $\overline{u'^2}$ at high Mach numbers. The acoustic-vortical part has a large contribution at the shock wave for $M_{\rm in} > 1.5$, and represents the correlation between the dilatational and solenoidal components of the streamwise velocity fluctuations. The acoustic-acoustic part of $\overline{u'^2}$ is comparatively lower for high Mach numbers, as observed for the $\overline{u'T'}$ and $\overline{T'^2}$ correlations.

In summary, it is clear that R_{uT} has significant contributions from the acoustic mode at low Mach numbers. By comparison, the vorticity and entropy modes are the dominant contributors to R_{uT} for strong shock waves. Note that the results presented in figure 8 corresponds to the $x = 0$ location, immediately behind the shock. The energy in the acoustic mode decays to low values farther

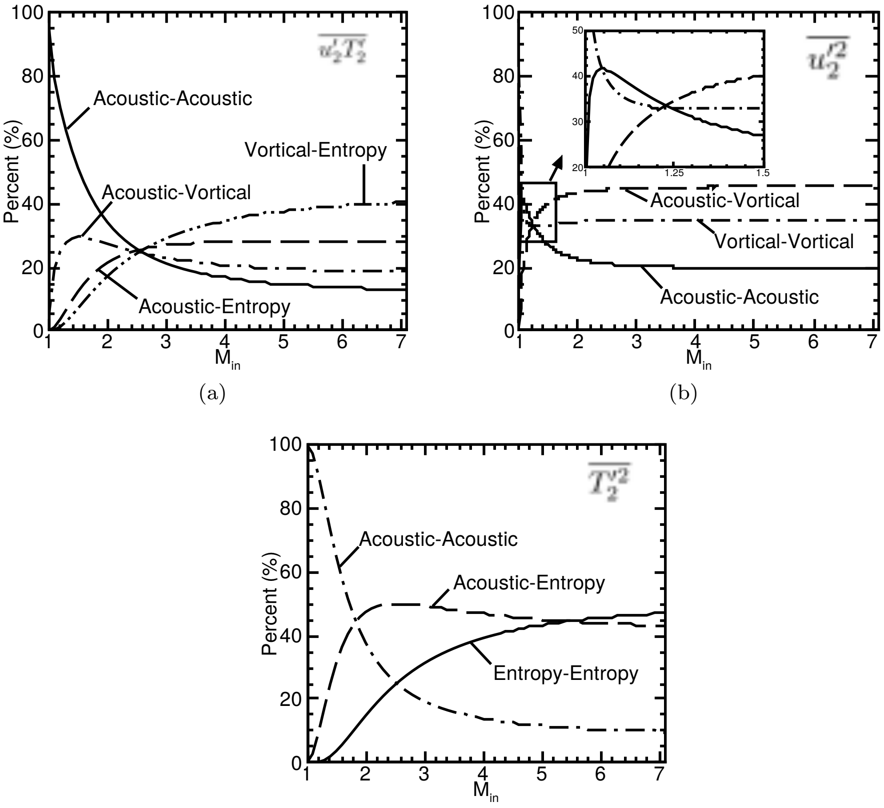

(c)

Fig. 8 Percentage contribution of the Kovasznay components to the near-field ($x = 0$) values of (a) $\overline{u'T'}$, (b) $\overline{u'^2}$ and (c) $\overline{T'^2}$, as predicted by LIA for purely vortical incoming disturbances.

away from the shock, and thus the far-field values of $\overline{u'T'}$, $\overline{u'^2}$, $\overline{T'^2}$ and R_{uT} are primarily composed of the vortical and entropy components, at all Mach numbers.

3.3 Comparison of individual modes

For a given upstream turbulence that is purely vortical, we now know the dominant downstream modes that contribute to R_{uT}, both a function of Mach number and distance from the shock wave. We compare the individual downstream modes between LIA and DNS to explain the similarities and differences between the LIA and DNS R_{uT} values presented in section 3.1.

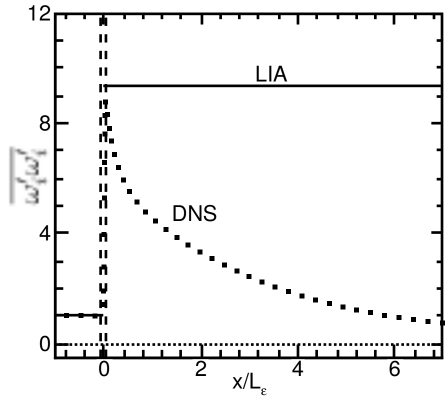

Fig. 9 Streamwise evolution of the enstrophy $\overline{\omega_i'\omega_i'}$ as predicted by LIA (line; purely vortical incoming disturbances) and DNS (symbols) for the case of $M_{\text{in}} = 3.5$. The DNS data corresponds to $Re_{\lambda,\text{in}} = 40$ and $M_{t,\text{in}} = 0.15$, and the two vertical lines show the region of shock oscillation in the simulation. The correlations are normalized by their respective values just upstream of the shock.

3.3.1 The vorticity mode

For incident isotropic disturbances, the upstream enstrophy is given by [11]

$$\frac{\left(\overline{\omega_i'\omega_i'}\right)_1}{U_1^2} = 3\int_{\psi=0}^{\pi/2} (2-\sin^2\psi)\sin\psi\,\mathrm{d}\psi \int_{k=0}^{\infty} \frac{k^2 E(k)}{2}\mathrm{d}k, \tag{11}$$

where ω' is the fluctuating vorticity, and $E(k)$ is given by (5). The shock-normal vorticity variance remains unaffected across the shock, but the shock-transverse components get amplified. The post-shock value of the enstrophy can be computed using

$$\begin{aligned}\frac{\left(\overline{\omega_i'\omega_i'}\right)_2}{U_1^2} =& \frac{1}{3}\frac{\left(\overline{\omega_i'\omega_i'}\right)_1}{U_1^2} + 2\int_{\psi=0}^{\pi/2} \left(r^2\,\cos^2\psi\left|\hat{I}\right|^2 + \sin^2\psi\,\left|\hat{G}\right|^2 - \right.\\ &\left. 2r\,\cos\psi\,\sin\psi(\hat{I}_r\hat{G}_r + \hat{I}_i\hat{G}_i) + r^2\,\cos^2\psi\right)\sin\psi\,\mathrm{d}\psi \times \int_{k=0}^{\infty}\frac{k^2E(k)}{2}\mathrm{d}k,\end{aligned} \tag{12}$$

where $\hat{G}$ and $\hat{I}$ represent the complex coefficients in (6), and subscripts r and i correspond to their real and imaginary parts.

A sample result is shown in figure 9, where the post-shock enstrophy is constant as per the linear inviscid theory. The DNS data, on the contrary, shows a rapid viscous decay behind the shock. The near-field values (extrapolated to the mean shock location in DNS [22, 5]) are compared in figure 10, showing an excellent match between LIA and DNS. Similar results were presented by Sinha [21]; an exception is the Mach 3.5 case at $Re_{\lambda,\text{in}} = 75$, which may require

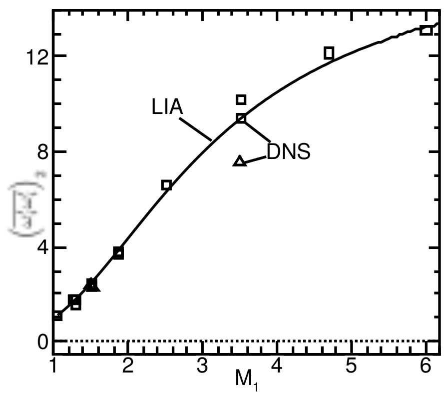

Fig. 10 Post-shock enstrophy in the near-field (at $x = 0$) by LIA (line; purely vortical incoming disturbances) and DNS (symbols), normalized by the upstream value. The DNS cases are grouped into $Re_{\lambda,\mathrm{in}} = 40$ (square) and $Re_{\lambda,\mathrm{in}} = 75$ (triangle).

further grid refinement in the simulation. Thus the change in enstrophy across the shock is governed by a linear inviscid mechanism, while the downstream evolution is clearly strongly affected by some combination of nonlinear (e.g., vortex stretching or return-to-isotropy of the vorticity vector) and viscous effects. At high Mach numbers, the post-shock peak R_{uT} observed in the region $0 < x/L_\epsilon < 1$ has large contribution from the vortical mode (see figure 8). The discrepancies between DNS and LIA due to the missing nonlinear and viscous effects could then lead to potentially significant differences in the predicted peak R_{uT}, as well.

3.3.2 The entropy mode

The linearized expression for the normalized entropy fluctuation is

$$\frac{s'}{c_p} = \frac{p'}{\gamma \overline{p}} - \frac{\rho'}{\overline{\rho}}, \tag{13}$$

where c_p is the specific heat at constant pressure. In LIA, an expression for the downstream entropy variance for incoming isotropic turbulence is

$$\overline{s_2'^2} = 4\pi \int_{k=0}^{\infty} \int_{\psi=0}^{\pi/2} \left(\overline{s_2'^2}\right)_{2D} k^2 \sin\psi \, \mathrm{d}\psi \, \mathrm{d}k, \tag{14}$$

where $\left(\overline{s_2'^2}\right)_{2D} = \overline{s_2' s_2'^*}$ represents the entropy variance obtained for a two-dimensional interaction, which can be computed using the p_2' and ρ_2' expressions given in (6).

The DNS and LIA results for the entropy variance in figure 11 are qualitatively similar to the enstrophy data presented previously. The rapid viscous decay in DNS is not captured by the LIA predictions, but there is a close

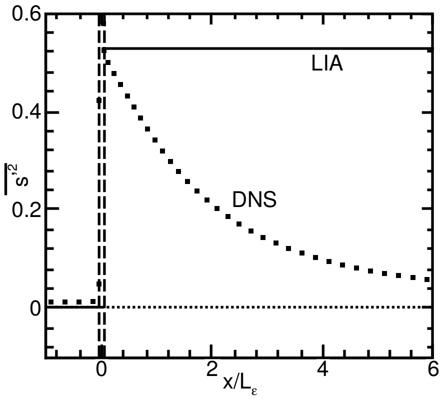

Fig. 11 Streamwise variation of the entropy variance $\overline{s'^2}$ for the case of $M_{\rm in} = 3.5$ as predicted by LIA (line; purely vortical incoming disturbances) and DNS (symbols), where DNS has $Re_{\lambda,\rm in} = 40$ and $M_{t,\rm in} = 0.15$. The entropy fluctuations are normalized by c_p and the velocity fluctuations are normalized by the upstream mean velocity. The correlation is further normalized by the upstream TKE.

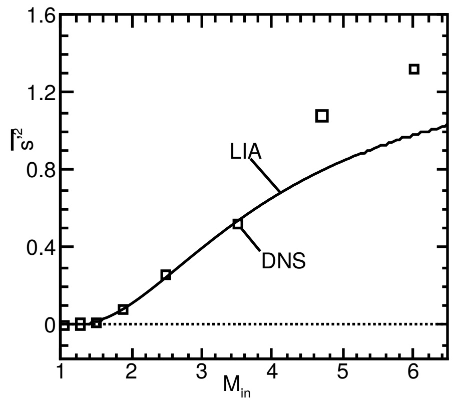

Fig. 12 Amplification of $\overline{s'^2}$ across the shock for varying upstream Mach number as predicted by LIA (purely vortical incoming disturbances) and DNS (symbols). The DNS cases correspond to the lowest $M_{t,\rm in}$ value for a given upstream Mach number. Normalization as described in figure 11.

match between the LIA near-field value and the DNS data extrapolated to the shock wave. This is true for Mach numbers up to 3.5 (see figure 12), beyond which the DNS entropy variance is higher than the theoretical prediction. A possible reason is that the incoming turbulence in DNS is not purely vortical, but has finite thermodynamic fluctuations [5]. These fluctuations could affect the downstream correlations especially at higher Mach numbers [11, 4].

The data suggests that the generation of the entropy mode across the shock is governed by linear mechanisms, while the downstream evolution is significantly affected by viscous and nonlinear mechanisms. This is similar to the vorticity mode, and can directly lead to the LIA-DNS mismatch in the peak R_{uT} at higher Mach numbers, where there is a significant contribution from the vorticity-entropy components.

3.3.3 The acoustic mode

As modelled in LIA, the pressure fluctuations have contributions solely from the acoustic mode. We compare the pressure-variance between LIA and DNS to comment on the acoustic mode behaviour. The pressure variance for three-dimensional incoming turbulence can be written as [11]

$$\overline{p_2'^2} = 4\pi \int_{k=0}^{\infty} \int_{\psi=0}^{\pi/2} \left(\overline{p_2'^2}\right)_{2D} k^2 \sin\psi \,\mathrm{d}\psi \,\mathrm{d}k, \tag{15}$$

where $\left(\overline{p_2'^2}\right)_{2D} = \overline{p_2' p_2'^*}$ represents the pressure variance obtained for a two-dimensional interaction, and can be computed using the expression given in (6).

We use the linearized Euler equations to derive a transport equation for the pressure variance downstream of the shock.

$$\frac{D}{Dt}\left(\frac{\overline{p'^2}}{2}\right) = -2\gamma\overline{p}\; \overline{p' \frac{\partial u_j'}{\partial x_j}}, \tag{16}$$

where the left-hand side represents the material derivative and $\partial u_j'/\partial x_j$ is the fluctuating dilatation. The pressure variance thus varies along the streamwise direction in the linear limit, unlike the vorticity and entropy variances, and its rate of change is governed by the pressure-dilatation correlation.

Figure 13 shows the streamwise evolution of the pressure variance obtained from DNS and LIA for two Mach numbers. There is an exponential decay immediately behind the shock that is well predicted by LIA. In the far-field, the linear theory gives a constant level associated with the propagating acoustic waves. The DNS results are in good agreement with this, but with a slight decay. The decay is much less pronounced compared to the vorticity- and entropy-results, which must be due to the much larger length scales for the acoustic waves. Note that there is a clear increase in the far-field value at the higher Mach number.

The DNS data shows an excellent match with the LIA far-field predictions for the entire range of Mach numbers (figure 14). The near-field results also compare well, within the constraints of accurately extrapolating the DNS data back to the shock center, due to the extremely rapid decay behind the shock (and the finite region of shock oscillation). This was found to be particularly difficult at low Mach numbers, which is why those cases are absent in the figure. Overall, it is found that LIA can accurately predict the generation of acoustic energy at the shock, its decay behind the shock, and the propagation of sound waves into the far-field. At low Mach numbers, the rapid variation in R_{uT} close to the shock is governed by the acoustic mode (see figure 8). This

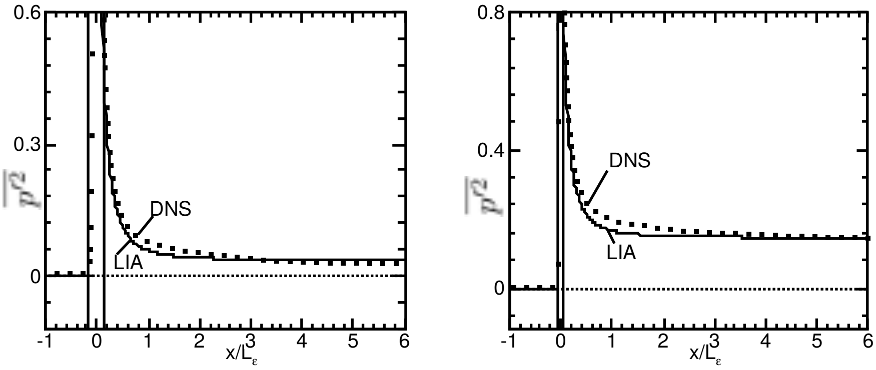

(a) (b)

Fig. 13 Streamwise variation of $\overline{p'^2}$ as predicted by LIA (line; purely vortical incoming disturbances) and DNS (symbols) for the case of (a) $M_{\rm in} = 1.50$ and (b) $M_{\rm in} = 3.5$. The DNS data correspond to $Re_{\lambda,\rm in} = 40$ and $M_{t,\rm in} = 0.15$. The pressure fluctuations are normalized by the downstream mean pressure and the velocity fluctuations are normalized by the upstream mean velocity. The correlation is further normalized by the upstream TKE.

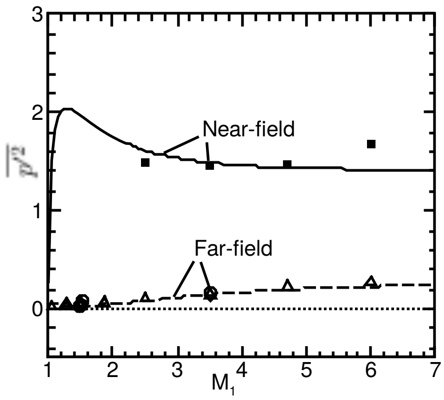

Fig. 14 Near-field and far-field values of $\overline{p'^2}$ for varying upstream Mach number in LIA (lines; purely vortical incoming disturbances) and DNS (symbols). The lowest $M_{t,\rm in}$ values at each Mach number and $Re_{\lambda,\rm in} = 40$ are considered for the near-field comparison, whereas all DNS cases listed in table 1 are considered for the far-field comparison, with $Re_{\lambda,\rm in} = 40$ (triangles) and $Re_{\lambda,\rm in} = 75$ (circles). The DNS far-field data is averaged over $4 \leq x/L_\epsilon \leq 6$. Normalization as described in figure 13.

may explain the good match in the DNS and LIA values of peak post-shock R_{uT} at low Mach numbers.

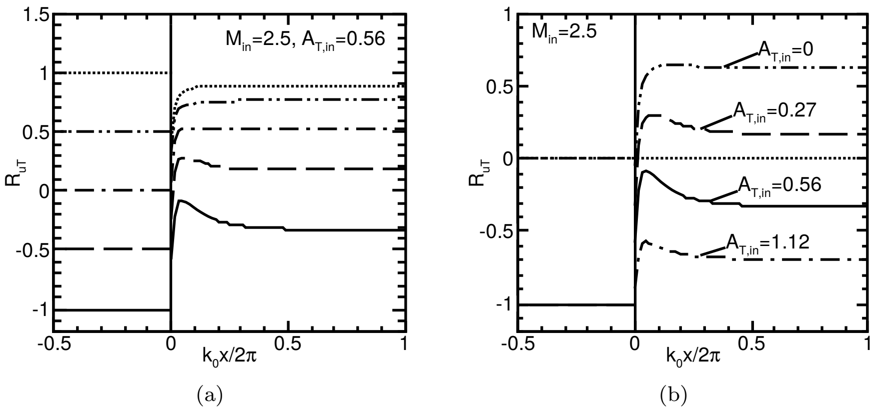

Fig. 15 Streamwise variation of R_{uT} when vorticity-entropy upstream turbulence interacts with a Mach 2.5 shock wave for (a) varying $R_{uT,\mathrm{in}}$ values: -1 (solid), -0.5 (dashed), 0 (dash-dotted), 0.5 (dash double-dotted) and 1 (dotted), with the amplitude ratio $A_{T,\mathrm{in}} = 0.56$, and (b) varying amplitude ratio for $R_{uT,\mathrm{in}} = -1$.

4 Post-shock R_{uT} for entropic and acoustic upstream turbulence

The LIA results presented so far are for purely vortical upstream turbulence. However, practical high-speed flows can have significant levels of entropy and acoustic fluctuations. In this section, we study the variation of R_{uT} across a shock when the upstream turbulence has entropy and acoustic fluctuations.

4.1 Combined vorticity-entropy upstream turbulence

We consider a field of vorticity and entropy waves interacting with a normal shock. The thermodynamic field is related to the velocity fluctuations by [24]

$$\frac{\rho'}{\overline{\rho}} = -\frac{T'}{\overline{T}} = A_{T,\mathrm{in}} \exp(i\phi_{T,\mathrm{in}}) \frac{u'}{U},$$

and the pressure fluctuations are neglected. Here, $A_{T,\mathrm{in}}$ can be interpreted as the ratio of the normalized temperature and velocity fluctuations in the incoming flow, and $\phi_{T,\mathrm{in}}$ is the corresponding phase difference. The velocity-temperature correlation coefficient in the incoming flow is thus given by $R_{uT,\mathrm{in}} = -\cos\phi_{T,\mathrm{in}}$. Morkovin's hypothesis corresponds to taking $A_{T,\mathrm{in}} = (\gamma - 1)M_{\mathrm{in}}^2$ and $R_{uT,\mathrm{in}} = -1$. The procedure for calculating the downstream disturbance field is similar to that described in section 2 with details available in Mahesh et al [11]. Note that amplitude and phase difference are applied to each elementary wave, which results in an axisymmetric incoming entropy field.

Figure 15(a) shows the streamwise variation of R_{uT} for the upstream values of the correlation ranging from -1 to +1. The case with $R_{uT,\mathrm{in}} = 0$ results in a positive velocity-temperature correlation behind the shock, and the streamwise

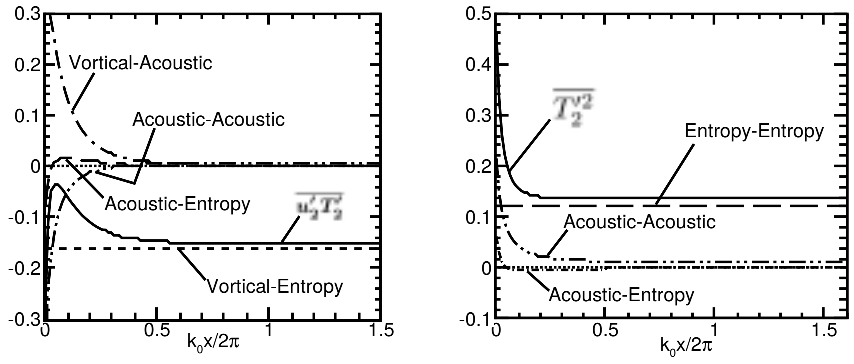

(a) (b)

Fig. 16 Kovasznay mode decomposition of (a) $\overline{u'T'}$ and (b) $\overline{T'^2}$ for a vorticity-entropy disturbance field interacting with a shock wave at $M_{\rm in} = 2.5$. The shock is located at $x = 0$. The upstream turbulence is characterised by $A_{T,\rm in} = 0.56$ and $R_{uT,\rm in} = -1$. Normalization as described in figure 7.

variation is akin to that presented in figure 4(a). The post-shock values are relatively lower for negative $R_{uT,\rm in}$, whereas higher values are attained for positively correlated velocity-temperature fluctuations in the incoming flow. All the cases exhibit a rapid variation of R_{uT} downstream of the shock wave similar to the purely vortical interaction (see figure 4(a)).

The effect of varying upstream amplitude ratio on the correlation coefficient is presented in figure 15(b). As $A_{T,\rm in}$ increases, the post-shock R_{uT} decreases and takes negative values for high levels of upstream entropy fluctuations. This is true for $R_{uT,\rm in} = -1$. An opposite trend is observed for $R_{uT,\rm in} > 0$, and we find positively correlated velocity and temperature fluctuations behind the shock. Note that the sign of the correlation determines the direction of heat transfer due to turbulent mixing. Positive values of R_{uT} indicate heat transfer away from the shock, whereas a negative correlation coefficient implies that the turbulent heat transfer is directed towards the shock wave.

Figure 16 shows the Kovasznay mode decomposition of $\overline{u'T'}$ and $\overline{T'^2}$ for $M_{\rm in} = 2.5$, $A_{T,\rm in} = 0.56$ and $R_{uT,\rm in} = -1$. The acoustic contributions to $\overline{u'T'}$ are qualitatively similar to those in figure 7(a), with large post-shock magnitudes and a decay within $k_0x/2\pi = 0.5$. The vortical-entropy component in this case is negative, unlike that in the purely vortical interaction, and it leads to a negative far-field value of $\overline{u'T'}$. The rapid post-shock variation and the local peak in $\overline{u'T'}$ is a result of the acoustic adjustment behind the shock wave. Similar observations can be made for $\overline{T'^2}$ in figure 16(b), where the acoustic contributions are large immediately behind the shock, and the far-field is dominated by the entropy mode. The modal decomposition of $\overline{u'^2}$ exhibits identical trends to that in figure 7(b), and is not shown here. Overall, the three turbulent correlations contributing to R_{uT} are dominated by the acoustic mode in the vicinity of the shock wave. The linear theory is therefore

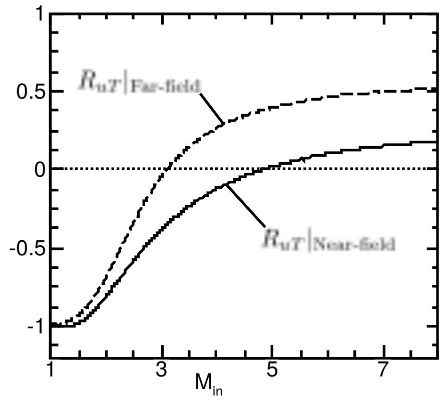

Fig. 17 Near-field and far-field R_{uT} as predicted by LIA for varying upstream Mach number. The upstream turbulence has vorticity-entropy fluctuations with amplitude ratio $A_{T,\mathrm{in}} = 0.56$ and $R_{uT,\mathrm{in}} = -1$.

expected to well predict the near-field R_{uT} and its rapid variation behind the shock.

The LIA predictions of the near-field and the far-field R_{uT} are plotted in figure 17 for a range of upstream Mach numbers. As expected, the downstream R_{uT} is close to its upstream value of -1 for very weak shock waves ($M_{\mathrm{in}} \to 1$). The correlation coefficient increases with Mach number to take positive values for strong shock waves. The far-field R_{uT} is primarily due to the vorticity-entropy contribution, while the near-field value is dominated by the acoustic mode. The difference between the far-field and the near-field R_{uT} is the net acoustic contribution to the correlation coefficient. A large difference at high Mach numbers thus indicates a higher acoustic contribution close to the shock, as compared to the low Mach number interactions.

4.2 Purely acoustic upstream field

We next study the interaction of a field of acoustic waves with a normal shock by following the procedure outlined by Moore [13]. The acoustic and the vorticity/entropy waves travel at different speed upstream of the shock and are not correlated to each other. Therefore, R_{uT} generated by the combined field of the acoustic and vorticity/entropy waves can be analyzed by first studying the independent interaction of the acoustic waves with the shock. The combined value of R_{uT} can then be calculated based on the ratio of dilatational turbulence kinetic energy associated with the acoustic mode to the total turbulence kinetic energy in the flow field. Details are provided in Mahesh et al [10].

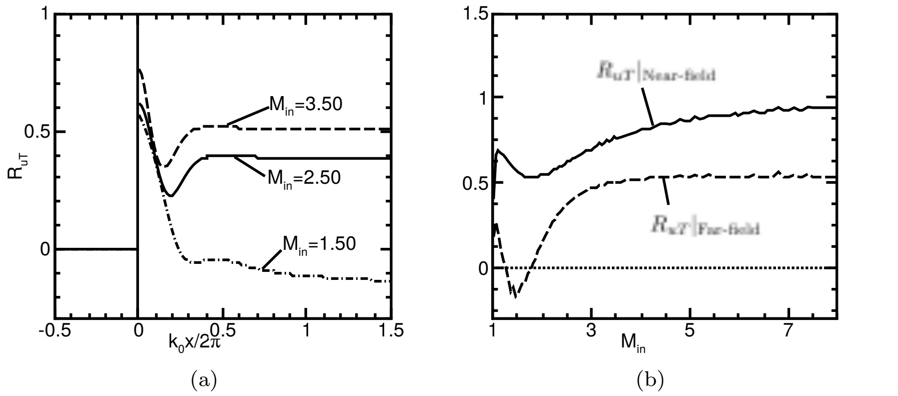

Fig. 18 R_{uT} values obtained by the interaction of a purely acoustic disturbance field with a normal shock. (a) Streamwise variation of R_{uT} for three Mach numbers, with $x = 0$ representing the shock location. (b) Near-field and far-field values of R_{uT} for varying upstream Mach numbers.

An acoustic wave interacting with a stationary shock wave is given by

$$\frac{u_1'}{U_1} = -\frac{\cos\psi}{\gamma M_{\text{in}}} A_p \exp[ik(x\cos\psi + y\sin\psi - (U_1\cos\psi + a_1)t)], \tag{17a}$$

$$\frac{v_1'}{U_1} = \frac{\sin\psi}{\gamma M_{\text{in}}} A_p \exp[ik(x\cos\psi + y\sin\psi - (U_1\cos\psi + a_1)t)], \tag{17b}$$

$$\frac{T_1'}{\overline{T}_1} = \frac{\gamma - 1}{\gamma} A_p \exp[ik(x\cos\psi + y\sin\psi - (U_1\cos\psi + a_1)t)], \tag{17c}$$

where A_p represents the amplitude of the upstream pressure fluctuations. The LIA procedure is similar to that presented in section 2. The downstream solution is more involved, and is given in Mahesh et al [10]. Three-dimensional results obtained by integrating the two-dimensional results over the von Karman spectrum given in (5) are presented below.

Figure 18(a) shows the LIA predictions for different upstream Mach numbers. It is found that the downstream variation of R_{uT} generated by the upstream acoustic field is qualitatively different from those in the purely vortical and the vorticity-entropy cases. Specifically, R_{uT} takes a large positive value immediately behind the shock and rapidly decays to lower asymptotic values in the far-field. The near-field and the far-field values also show a non-monotonic variation with Mach number, unlike earlier cases (figures 4(b) and 17). Also, the far-field R_{uT} values are lower than the near-field values for all Mach numbers indicating a net positive contribution of the decaying acoustic component behind the shock wave.

The modal decomposition of $\overline{u'T'}$, $\overline{u'^2}$ and $\overline{T'^2}$ (figure 19) shows interesting trends. The post-shock $\overline{T'^2}$, both near-field and far-field, are determined by the acoustic components. Same is true for $\overline{u'T'}$ and $\overline{u'^2}$. Also, the streamwise variation of $\overline{u'T'}$ and $\overline{u'^2}$ for this case is qualitatively different from those

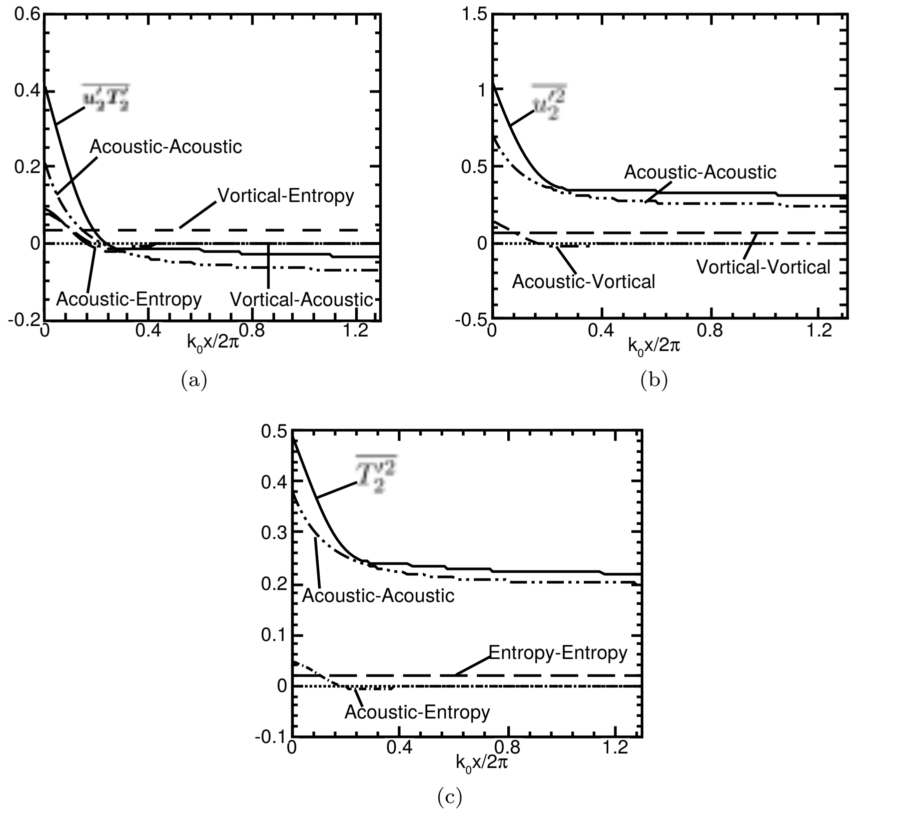

Fig. 19 Kovasznay mode decomposition of (a) $\overline{u'T'}$, (b) $\overline{u'^2}$ and (c) $\overline{T'^2}$ for a purely acoustic disturbance field interacting with a normal shock. The upstream Mach number is $M_{\rm in} = 1.50$, and the shock is located at $x = 0$. Normalization as described in figure 7.

observed in figure 7 and 16. Overall, all the turbulent correlations contributing to the post-shock R_{uT} are dominated by the acoustic components, and hence are expected to be predicted well by LIA. This is true for acoustic disturbance field interacting with weak shocks. A similar decomposition carried out for stronger shock waves (data not shown) reveals that the vorticity and entropy modes can have significant contribution to post-shock R_{uT} at higher Mach numbers.

5 Summary

In this work, we investigate the correlation coefficient R_{uT} between the streamwise velocity and the temperature in a canonical shock-turbulence interaction. Linear interaction analysis (LIA) is employed to predict the post-shock values for vortical, acoustic and entropic upstream turbulence field. The predictions

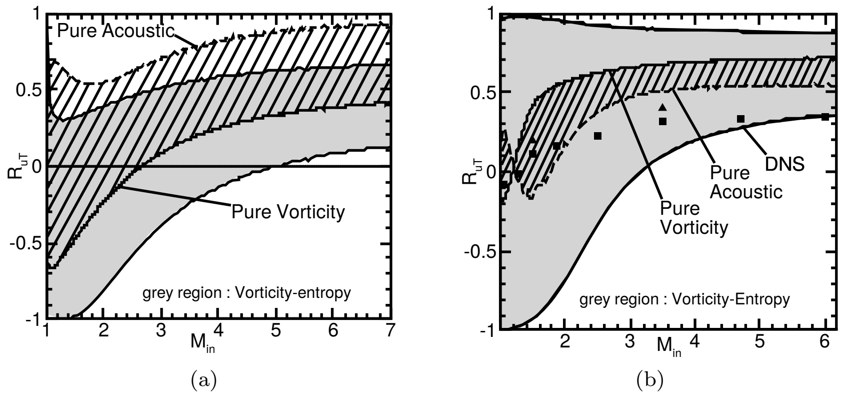

Fig. 20 Summary of LIA predictions for the R_{uT} correlation coefficient in the (a) near-field at $x = 0$ and (b) far-field at $x \to \infty$. The grey region shows the bounds (for different phase angles) for combined vorticity-entropy incoming disturbances for an amplitude ratio of $A_{T,\mathrm{in}} = 0.56$. The hatched region corresponds to different amplitude ratios of incoming vorticity and acoustic disturbances having the same spectrum. The DNS results in the far-field (averaged over $2 < x/L_\epsilon < 6$) are for the lowest $M_{t,\mathrm{in}}$ at each M_{in}, at $Re_{\lambda,\mathrm{in}}$ of 40 (squares) and 75 (triangles). Note that the DNS results are known to be low due to the low Reynolds number, as evidenced in Fig. 6.

are then compared to available DNS data for which the incoming turbulence was mostly vortical. The results are summarized in figure 20.

For purely vortical upstream turbulence, LIA predicts a far-field R_{uT} that increases with the shock strength. The DNS data is in qualitative agreement but with lower quantitative values. This is most likely due to the known effect of the Reynolds number: e.g., note that the $Re_{\lambda,\mathrm{in}} = 75$ results are consistently higher than those at 40. The addition of acoustic incoming waves increases the near-field R_{uT} but generally (for $M_{\mathrm{in}} \gtrsim 1.2$) decreases the far-field R_{uT}. The addition of incoming entropy waves can increase or decrease the R_{uT} values depending on their correlation with the incoming vorticity. For the important special case of $R_{uT,\mathrm{in}} = -1$ (which corresponds to each elementary wave satisfying Morkovin's hypothesis), the addition of incoming entropy waves leads to decreased post-shock R_{uT} values.

The downstream R_{uT} obtained for purely vortical upstream turbulence is decomposed in terms of the Kovasznay modes of vorticity, entropy and acoustics. The vorticity-entropy downstream mode has a large contribution to the velocity-temperature correlation generated by strong shock waves. These modes are strongly influenced by viscous and non-linear effects, which explains the mismatch between LIA and DNS at high Mach numbers. At low Mach numbers, the acoustic downstream mode dominates the disturbance field behind the shock, and the peak R_{uT} value is determined by the acoustic decay in this region. There is a close match between the LIA prediction and the DNS data in terms of the generation and downstream evolution of the acoustic mode, and thus the peak positive R_{uT} generated by the vortical disturbance field interacting with relatively weak shocks is well predicted by LIA. The acoustic mode is also found to be dominant for weak shock interactions of upstream turbulence with entropy and acoustic disturbances, and thus LIA is expected to provide reasonably accurate predictions of R_{uT} in such cases. Well-validated LIA predictions, along with DNS data, can thus be effectively used to propose new models for the turbulent heat flux in shock-dominated flows.

Acknowledgements

The authors wish to acknowledge the contributions of Yogesh Prasaad, a graduate student, under the supervision of the second author. He helped with formulation pertaining to section 4. The first and second authors would like to thank Indian Space Research Organisation-Space Technology Cell (ISRO-STC) and Aeronautics Research and Development Board (ARDB) for supporting this research. The third author is supported by the National Science Foundation, grant CBET-1453633.

References

1. Fabre D, Jacquin L, Sesterhenn J (2001) Linear interaction of a cylindrical entropy spot with a shock. Phys Fluids 13(8):2403–2422
2. Haidinger FA, Friedrich R (1993) Computation of shock wave/turbulent boundary layer interactions using a two-equation model with compressibility corrections. Flow, Turbulence and Combustion 51:501–505
3. Hannappel R, Friedrich R (1995) Direct numerical simulation of a mach 2 shock interacting with isotropic turbulence. Appl Sci Res 54:205221
4. Jamme S, Cazalbou JB, Torres F, Chassaing P (2002) Direct numerical simulation of the interaction between a shock wave and various types of isotropic turbulence. Flow, Turbulence and Combustion 68:227–268
5. Larsson J, Lele SK (2009) Direct numerical simulation of canonical shock-turbulence interaction. Phys Fluids 21:126,101
6. Larsson J, Bermejo-Moreno I, Lele SK (2013) Reynolds- and Mach number effects in canonical shock-turbulence interaction. J Fluid Mech 717:293–321
7. Lee S, Lele SK, Moin P (1993) Direct numerical simulation of isotropic turbulence interacting with a weak shock wave. J Fluid Mech 251:533–562
8. Lee S, Lele SK, Moin P (1997) Interaction of isotropic turbulence with shock waves: effect of shock strength. J Fluid Mech 340:225–247
9. Loyau H, Batten P, Leschziner MA (1998) Modelling shock/boundary-layer interaction with nonlinear eddy-viscosity closures. Flow, Turbulence and Combustion 60:257–282
10. Mahesh K, Lee S, Lele SK, Moin P (1995) The interaction of an isotropic field of acoustic waves with a shock wave. J Fluid Mech 300:383–407

11. Mahesh K, Lele SK, Moin P (1996) The interaction of a shock wave with a turbulent shear flow. Tech. Rep. 69, Thermosciences division, Department of Mechanical Engineering, Stanford University, Stanford, CA.
12. Mahesh K, Lele SK, Moin P (1997) The influence of entropy fluctuations on the interaction of turbulence with a shock wave. J Fluid Mech 334:353–379
13. Moore FK (1954) Unsteady oblique interaction of a shock wave with a plane disturbance. Tech. Rep. 2879, NACA Report
14. Morkovin MV (1962) Effects of compressibility on turbulent flows. Mecanique de la Turbulence, CNRS edited by A Favre, Gordon and Breach, New York, pp 367–380
15. Pope SB (2000) In: Turbulent Flows, Cambridge Univ. Press, London
16. Quadros R, Sinha K, Larsson J (2016) Turbulent energy flux generated by shock/homogeneous-turbulence interaction. Submitted to J Fluid Mech
17. Ribner HS (1953) Convection of a pattern of vorticity through a shock wave. Tech. Rep. 2864, NACA TN
18. Ribner HS (1954) Shock-turbulence interaction and the generation of noise. Tech. Rep. 1233, NACA Report
19. Roy CJ, Blottner FG (2001) Review and assessment of turbulence models for hypersonic flows. Progress in Aerospace Sciences 42 (7):469–530
20. Ryu J, Livescu D (2014) Turbulence structure behind the shock in canonical shock-vortical turbulence interaction. J Fluid Mech 756:R1
21. Sinha K (2012) Evolution of enstrophy in shock/homogeneous turbulence interaction. J Fluid Mech 707:74–110
22. Sinha K, Mahesh K, Candler GV (2003) Modeling shock-unsteadiness in shock-turbulence interaction. Phys Fluids 15:2290–2297
23. Smits AJ, Dussauge JP (2006) In: Turbulent shear layers in supersonic flow, Springer, USA
24. Veera VK, Sinha K (2009) Modelling the effect of upstream temperature fluctuations on shock/homogeneous turbulence interaction. Phys Fluids 21:025,101
25. Xiao X, Hassan HA, Edwards JR, Jr RLG (2007) Role of turbulent Prandtl numbers on heat flux at hypersonic Mach numbers. AIAA Journal 45 (4):806–813